Effects of trapped electrons on ion reflection in an oblique shock wave

Cite as: Phys. Plasmas **22**, 062305 (2015); https://doi.org/10.1063/1.4922847
Submitted: 15 April 2015 • Accepted: 03 June 2015 • Published Online: 23 June 2015

Mieko Toida and Junya Inagaki

Effects of trapped electrons on ion reflection in an oblique shock wave

Mieko Toida[1,a)] and Junya Inagaki[2]
[1]National Institute for Fusion Science, Toki 509-5292, Japan
[2]Department of Physics Nagoya University, Nagoya 464-8602, Japan

(Received 15 April 2015; accepted 3 June 2015; published online 23 June 2015)

A magnetosonic shock wave propagating obliquely to an external magnetic field can trap electrons and accelerate them to ultrarelativistic energies. The trapped electrons excite two-dimensional (2D) electromagnetic fluctuations with finite wavenumbers along the shock front. We study effects of the trapped electrons on ion motions through the 2D fluctuations. It is analytically shown that the fraction of ions reflected from the shock front is enhanced by the 2D fluctuations. This is confirmed by 2D (two space coordinates and three velocities) relativistic, electromagnetic particle simulations with full ion and electron dynamics and calculation of test ions in the electromagnetic fields averaged along the shock front. A comparison between 2D and one-dimensional electromagnetic particle simulations is also shown. © *2015 AIP Publishing LLC*.
[http://dx.doi.org/10.1063/1.4922847]

I. INTRODUCTION

Electromagnetic particle simulations with full ion and electron dynamics have shown that a large-amplitude magnetosonic shock wave can promptly accelerate ions and electrons with different nonstochastic mechanisms caused by strong electromagnetic fields in the shock wave (Ref. 1 and references therein). For example, some ions are accelerated via reflection by magnetic and electrostatic fields at the shock front.[2–4] In Ref. 5, it was shown that energies of reflected ions can be relativistic if the external magnetic field is strong such that $|\Omega_e|/\omega_{pe} > 1$, where $\Omega_e(< 0)$ and ω_{pe} are electron gyro and plasma frequencies, respectively. It was also pointed out that this mechanism can explain the observations of acceleration of solar energetic protons reported in Refs. 6 and 7.

Electrons are accelerated by a different mechanism. A magnetosonic shock wave propagating obliquely to an external magnetic field can trap electrons and accelerate them.[8] The energies of the accelerated electrons can be ultrarelativistic such that $\gamma > 100$, where γ is the Lorentz factor, when $|\Omega_e|/\omega_{pe} > 1$ and the propagation speed of the shock wave v_{sh} is close to $c\cos\theta$, where c is the speed of light and θ is the propagation angle of the shock wave.[9] In such a wave, some electrons can be reflected near the end of the main pulse of a shock wave. Here, "main pulse" designates the first leading pulse in a shock wave (the shock wave approximates the train of solitons with damping amplitudes if the dissipation is small[4]). The reflected electrons are then trapped in the main pulse and are accelerated by the strong electric field there; the acceleration mechanism was described in detail in Ref. 8.

The trapped electrons significantly influence electromagnetic fields in a shock wave, which affect the motions of the trapped electrons. In the one-dimensional (1D) electromagnetic particle simulations,[10] the trapped electrons strengthen $E_\parallel$ and F, where $E_\parallel$ is the electric field parallel to the magnetic field and F is its integral along the magnetic field, $F = -\int E_\parallel ds$ with ds being the infinitesimal length along $\boldsymbol{B}$. This can cause the electrons to be trapped deeper in the main pulse. In the two-dimensional (2D) simulations,[11] the trapped electrons excite whistler-wave instabilities through interaction with whistler waves with finite wavenumbers along the shock front. As a result of nonlinear development of the instabilities, the 2D electromagnetic fluctuations along the shock front grow to large amplitudes. The 2D electromagnetic fluctuations can cause detrapping of energetic electrons from the main pulse and subsequent acceleration to much higher energies.[12]

In the above works, the interactions between the reflected ions and the trapped electrons were not investigated although both the electron and ion dynamics were calculated in the simulations. In a low beta plasma with $|\Omega_e|/\omega_{pe} > 1$, the fraction of the reflected ions is quite small because v_{sh} is much greater than the ion thermal velocity. Further, the reflected ions do not stay near the shock front, unlike the trapped electrons. Therefore, the effects of reflected ions on electromagnetic fields in a shock wave would be small, compared to those of trapped electrons that can stay near the shock front for a long period of time. In this paper, we study how ions are influenced by the electromagnetic fields that the trapped electrons produce. It is found that the number of reflected ions is increased because of the 2D electromagnetic fluctuations excited by the trapped electrons.

In Sec. II, we briefly describe the characteristics of electromagnetic fields and electron motion in an oblique shock wave for the 1D[10] and 2D[12] cases. In Sec. III, we analytically derive the condition for ions to be reflected from the shock front. It is predicted that the fraction of the reflected ions is enhanced by the 2D electromagnetic fluctuations. After describing the simulation model and parameters in Sec. IV, we study the effects of trapped electrons on ion motion in an oblique shock wave using 2D electromagnetic particle simulations in Sec. V. We follow the orbits of a large number of ions in the 2D simulation. We call these ions as 2Ds ions.

a)Electronic mail: toida.mieko@nifs.ac.jp

Furthermore, we calculate the orbits of the same number of test ions in the electromagnetic fields averaged along the shock front. That is, the test ions are not influenced by the 2D electromagnetic fluctuations. We call these test ions as 1Dt electrons. It is shown that the number of reflected 2Ds ions is greater than that of reflected 1Dt ions. Their difference increases with the amplitudes of the 2D electromagnetic fluctuations excited by the trapped electrons. We also perform 1D electromagnetic particle simulations. Although the trapped electrons strengthen $E_\parallel$ in the 1D case, the ion reflection is not significantly influenced by $E_\parallel$. Therefore, the fraction of reflected ions in the 1D case is smaller than that in the 2D case. Section VI gives a summary of our work.

II. EFFECTS OF TRAPPED ELECTRONS ON ELECTROMAGNETIC FIELDS IN THE SHOCK WAVE

We briefly describe effects of trapped electrons on electromagnetic fields in an oblique shock wave. We consider a magnetosonic shock wave propagating in the x direction with a constant speed v_{sh} in an external magnetic field in the (x, z) plane

$$\boldsymbol{B} = B_0(\cos\theta, 0, \sin\theta) = (B_{x0}, 0, B_{z0}). \tag{1}$$

Figure 1 shows the typical profiles of electromagnetic fields in an oblique shock wave with $v_{sh} \simeq c\cos\theta$. (These are obtained by the 2D electromagnetic particle simulation for the parameters in Sec. V. The profiles averaged over the period from $\omega_{pe}t = 1000$ to 3000 are plotted.) The main pulse region is $-15 < (x - x_m)/(c/\omega_{pe}) < 15$, where x_m is the position at which the magnetic field B_z becomes maximum. At $x \simeq x_m$, F also becomes maximum. The value of F can be

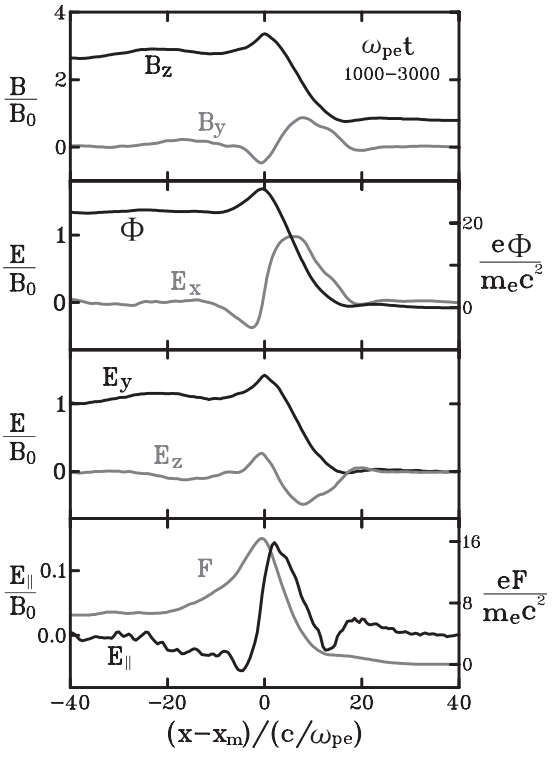

FIG. 1. Typical profiles of electromagnetic fields in an oblique shock wave.

greater than $m_e c^2$ when $|\Omega_e|/\omega_{pe} > 1$.[14] The time-averaged value of F is positive at the end of the main pulse. However, because of the fluctuations, F sometimes becomes negative. Then, some electrons can be reflected near the end of the main pulse and trapped in the main pulse region.[8]

The 1D particle simulation showed that as time advances, the number of trapped electrons increases.[13] The value of F at $x \simeq x_m$ also increases with time.[10] This was explained as follows. Assuming that the wave is 1D, we can approximate $E_\parallel$ and F in an oblique shock wave with $v_{sh} \simeq c\cos\theta$ as

$$E_\parallel = (E_x - B_y)B_{x0}/B, \tag{2}$$

$$F = \phi - \int_{x_0}^{x} dx B_y, \tag{3}$$

where ϕ is the electric potential and x_0 is a certain point in the far upstream region. The $E_\parallel$ and F are strengthened by trapped electrons. The electron velocity in the main pulse region can be approximated as

$$\boldsymbol{v} \simeq v_\parallel \frac{\boldsymbol{B}}{B} + c\frac{\boldsymbol{E}\times\boldsymbol{B}}{B^2}, \tag{4}$$

where $v_\parallel$ is the velocity parallel to $\boldsymbol{B}$. At $x = x_m$, v_z of a trapped electron becomes almost equal to c because $v_\parallel \simeq c$, $B_z \simeq B$, and the z component of the second term in Eq. (4) is almost zero. The trapped electrons form the current in the negative z direction, which produces the negative (positive) B_y in the region $x > x_m$ $(x < x_m)$. This strengthens $E_\parallel$ and F. The increase in F causes the electrons to be trapped deeper.[10]

The deep trapping can break down when multidimensional effects are considered. The 2D particle simulations demonstrated that the electromagnetic fluctuations with finite wavenumbers along the shock front can cause electron detrapping from the main pulse.[12] As described in Ref. 11, the 2D fluctuations begin to grow when the electron reflection near the end of the main pulse starts. The reflection changes the sign of the electron $v_\parallel$ from minus to plus, and the relative motion between reflected and incoming electrons excites whistler waves with $k_y \neq 0$ or $k_z \neq 0$ through Cherenkov resonance. In the case of the simulation plane (x, y) where the waves with $k_y \neq 0$ are included and those with $k_z \neq 0$ are excluded, oblique whistler waves with large θ_w are excited, where θ_w is the angle between the wavevector $\boldsymbol{k}$ and the ambient magnetic field. These waves generate density perturbations, which are roughly estimated as[12]

$$\frac{n_1}{n_0} \sim \tan\theta_w \frac{\omega_{pe}^2 ck}{|\Omega_e|(\omega_{pi}^2 + c^2k^2)}\frac{B_{1x}}{B_0}, \tag{5}$$

where n_1 and B_{1x} are perturbations of the density n and the magnetic field B_x, respectively. The density perturbation causes current filamentation; the current in the negative z direction is strong where the density of the trapped electrons is high. Because of the nonlinear interaction of the current filaments, the 2D fluctuations grow to large amplitudes. In the simulation plane (x, z) where the waves with $k_y \neq 0$ are

excluded and those with $k_z \neq 0$ are included, the whistler waves with small θ_w are excited. As suggested by Eq. (5), the density perturbations due to these waves are quite small, and the current filamentation is suppressed. Because of this, the amplitudes of the 2D fluctuations in the case of the simulation plane (x, z) are much smaller than those in the case of the simulation plane (x, y).[12] In the following, we consider the (x, y) plane for the 2D case and study how ions are influenced by the large-amplitude 2D fluctuations.

III. PHYSICAL CONSIDERATION FOR ION MOTION

We analytically discuss ion motion in an oblique shock wave. When ions encounter the shock wave, some ions can be reflected from the shock front. To obtain the amount of energy that reflected ions can gain, we need to use the relativistic equation of motion and consider the ion motions in electromagnetic fields that vary with x in the shock transition region. However, to qualitatively understand the reflection mechanism, we can use the nonrelativistic equation of motion. Further, according to Ref. 15 where ion reflection by a perpendicular shock wave was discussed, we use a simple model such that the electromagnetic fields are constant along x in the shock transition region.

A. Ion reflection by a 1D oblique shock wave

First, we analyze ion motion in a 1D oblique shock wave $(\partial/\partial y = \partial/\partial z = 0)$ in the wave frame (see Fig. 2), in which the upstream region is $x > x_1$, and the shock transition region (gray area) is $x_1 - \Delta < x < x_1$. The center of the main pulse x_m is equal to the left end of the transition region, $x_m = x_1 - \Delta$. We consider ions entering the transition region at $t = t_1$ with the velocity

$$\boldsymbol{v}_0 \simeq (-v_{sh} + \tilde{v}_x, \tilde{v}_y, \tilde{v}_z), \tag{6}$$

where $\tilde{\boldsymbol{v}}[= (\tilde{v}_x, \tilde{v}_y, \tilde{v}_z)]$ is due to thermal motion and $\tilde{v} \ll v_{sh}$ is assumed.

Assuming that $\boldsymbol{E}$ and $\boldsymbol{B}$ are constant in the shock transition region, we obtain the ion velocity v_x after $t = t_1$ as (for derivation, see the Appendix A)

$$v_x = V\cos[-\Omega(t - t_1) + \eta] + v_{gx} + \alpha_{\|x}(t - t_1). \tag{7}$$

Here, Ω is the ion cyclotron frequency in the transition region. V and η satisfy the relations

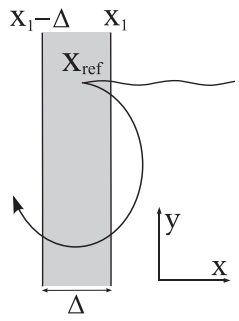

FIG. 2. Schematic representation of the orbit of a reflected ion in the wave frame. The gray area shows the shock transition region.

$$V\cos\eta = v_{x0} - v_{gx}, \tag{8}$$

$$V\sin\eta = \frac{cE_x}{B} - c\frac{B_x}{B^2}E_\| + \frac{B_z}{B}\tilde{v}_y - \frac{B_y}{B}\tilde{v}_z, \tag{9}$$

and v_{gx} and $\alpha_{\|x}$ are defined by

$$v_{gx} = c\frac{E_yB_z}{B^2} - c\frac{E_zB_y}{B^2} + \frac{B_x}{B}v_{\|0}, \tag{10}$$

$$\alpha_{\|x} = \frac{B_x}{B}\frac{q}{m}E_\|, \tag{11}$$

where $v_{\|0}$ is the parallel component of $\boldsymbol{v}_0$. From Eq. (7), the ion position x is written as

$$x - x_1 = -\frac{V}{\Omega}\sin[-\Omega(t - t_1) + \eta] + \frac{V}{\Omega}\sin\eta + v_{gx}(t - t_1) + \frac{\alpha_{\|x}}{2}(t - t_1)^2. \tag{12}$$

We now discuss the condition for ions to be reflected from the shock front. At the reflection point x_{ref}, v_x becomes zero. From Eq. (7), we can find that the reflection time t_{ref} satisfies the relation

$$V\cos(-\Omega\Delta t + \eta) + \alpha_{\|x}\Delta t = -v_{gx}, \tag{13}$$

where

$$\Delta t \equiv t_{ref} - t_1. \tag{14}$$

Then, from Eq. (12), we can write the reflection point x_{ref} as

$$x_{ref} - x_1 = -\frac{V}{\Omega}\sin(-\Omega\Delta t + \eta) + \frac{V}{\Omega}\sin\eta + v_{gx}\Delta t + \frac{\alpha_{\|x}}{2}\Delta t^2. \tag{15}$$

If the length $|x_{ref} - x_1|$ is shorter than the width of the shock transition region, $x_1 - x_{ref} < \Delta$, the particle would be reflected.

We assume that $|\Omega\Delta t| \ll 1$. Retaining terms of the order of $(\Omega\Delta t)^2$ in Eq. (13), we have

$$\Omega\Delta t \simeq \psi_0(1 + \delta), \tag{16}$$

where ψ_0 and δ are

$$\psi_0 \equiv -\frac{v_{gx} + V\cos\eta}{V\sin\eta + \alpha_{\|x}/\Omega}, \tag{17}$$

$$\delta \simeq \frac{V\cos\eta}{2\left(V\sin\eta + \alpha_{\|x}/\Omega\right)}\psi_0. \tag{18}$$

We can approximate δ as (for detail, see the Appendix)

$$\delta \simeq -\frac{v_{sh}^2}{2c^2}\frac{B^2}{E_x^2}, \tag{19}$$

where we have used $v_{sh} \gg |v_{gx}|, \tilde{v}$. (When the shock wave is stationary, $E_y = -v_{sh}B_{z0}/c$ and $E_z = 0$ in the wave frame. Therefore, we estimated $|v_{gx}| \sim v_{sh}B_{z0}/B$, which is much smaller than v_{sh} because $B \gg B_{z0}$.)

Substituting Eq. (16) in Eq. (15), we obtain the reflection point x_{ref} as

$$x_{\rm ref} - x_1 \simeq -\frac{(v_{gx} + V\cos\eta)^2}{2\Omega\left(V\sin\eta + \alpha_{\|x}/\Omega\right)}(1-\delta^2). \quad (20)$$

Then, by virtue of Eqs. (6), (8)–(11), and (19), the condition for ion reflection, $|x_{\rm ref} - x_1| < \Delta$, can be written as

$$\tilde{v}_x > v_{\rm ref}. \quad (21)$$

Here, $v_{\rm ref}$ is the minimum $\tilde{v}_x$ for the reflection and is given by

$$v_{\rm ref} = v_{\rm sh} - \sqrt{\frac{2qE_x\Delta}{m}}\left(1 + \frac{v_{\rm sh}^4}{8c^4}\frac{B^4}{E_x^4}\right), \quad (22)$$

where we have used $|B_y| \ll B_z$. Equation (22) indicates that E_x and B contribute the ion reflection and E_y, E_z, and $E_\|$ do not influence the ion motion. Using Eq. (21), we obtain the fraction of reflected particles as

$$\frac{n_{\rm ref}}{n_0} = \frac{1}{n_0}\int_{v_{\rm ref}}^{\infty} d\tilde{v}_x \int_{-\infty}^{\infty} d\tilde{v}_y \int_{-\infty}^{\infty} d\tilde{v}_z f(\tilde{\boldsymbol{v}}). \quad (23)$$

For a Maxwellian velocity distribution function

$$f(\tilde{\boldsymbol{v}}) = \frac{n_0}{\left(2\pi v_{Ti}^2\right)^{3/2}}\exp\left(-\frac{\tilde{v}^2}{2v_{Ti}^2}\right). \quad (24)$$

Eq. (23) leads

$$\frac{n_{\rm ref}}{n_0} = \frac{1}{2}{\rm erfc}\left(\frac{v_{\rm ref}}{\sqrt{2}v_{Ti}}\right), \quad (25)$$

where the complementary error function is defined as

$${\rm erfc(p)} = \frac{2}{\sqrt{\pi}}\int_p^{\infty} dt\exp(-t^2). \quad (26)$$

Equation (25) shows that $n_{\rm ref}/n_0$ increases as $v_{\rm ref}$ decreases. From Eq. (22), we see that $v_{\rm ref}$ decreases as E_x or B increases.

B. Reflection by a 2D shock wave

We now consider ion reflection by a 2D shock wave. We write the electric and magnetic fields as

$$\begin{aligned}\boldsymbol{E}(x,y,t) &= \bar{\boldsymbol{E}}(x,t) + \delta\boldsymbol{E}(x,y,t),\\ \boldsymbol{B}(x,y,t) &= \bar{\boldsymbol{B}}(x,t) + \delta\boldsymbol{B}(x,y,t),\end{aligned} \quad (27)$$

where $\bar{\boldsymbol{E}}$ and $\bar{\boldsymbol{B}}$ are defined as

$$\bar{\boldsymbol{E}} = \frac{1}{L_y}\int_0^{L_y} dy\boldsymbol{E}, \quad \bar{\boldsymbol{B}} = \frac{1}{L_y}\int_0^{L_y} dy\boldsymbol{B}, \quad (28)$$

which we call 1D averaged fields. We call $\delta\boldsymbol{E}$ and $\delta\boldsymbol{B}$ 2D fluctuations. In the following, we will show that the 2D fluctuations enhance the fraction of reflected ions.

In Sec. III A for the 1D shock wave, $\boldsymbol{E}$ and $\boldsymbol{B}$ were set to be constant in the shock transition region. In order to extend the consideration for the 1D case to the 2D case, we assume that $\boldsymbol{E}$ and $\boldsymbol{B}$ are constant in the limit of $\delta\boldsymbol{E}$ and $\delta\boldsymbol{B} \to 0$, that is, $\bar{\boldsymbol{E}}$ and $\bar{\boldsymbol{B}}$ are constant. As for the 2D fluctuations, we assume that $\delta\boldsymbol{E}$ and $\delta\boldsymbol{B}$ do not depend on x, which enables us to obtain the condition for the ion reflection analytically. We also assume that characteristic periods and wavelengths along y of the $\delta\boldsymbol{E}$ and $\delta\boldsymbol{B}$ are much longer than the period from t_1 to $t_{\rm ref}$ and the variation of the ion y during this period, respectively. This is consistent with the simulation result, which will be shown in Sec. V.

Under these assumptions, ions feel the constant electromagnetic fields in the shock transition region, although the values of $\boldsymbol{E}$ and $\boldsymbol{B}$ depend on the position y at which ions enter the shock transition region at $t = t_1$. Then, we may extend Eq. (22) to include a case in which $\boldsymbol{E}$ and $\boldsymbol{B}$ depend on y as

$$v_{\rm ref}(y) = v_{\rm sh} - \sqrt{\frac{2qE_x(y)\Delta}{m}}\left(1 + \frac{v_{\rm sh}^4}{8c^4}\frac{B(y)^4}{E_x(y)^4}\right). \quad (29)$$

Assuming that $|\delta\boldsymbol{E}|, |\delta\boldsymbol{B}| \ll |\bar{\boldsymbol{E}}|, |\bar{\boldsymbol{B}}|$, we can approximate Eq. (29) as

$$v_{\rm ref}(y) = \bar{v}_{\rm ref} + \delta v_{\rm ref}(y), \quad (30)$$

with

$$\bar{v}_{\rm ref} = v_{\rm sh} - \sqrt{\frac{2q\bar{E}_x\Delta}{m}}\left(1 + \frac{v_{\rm sh}^4}{8c^4}\frac{\bar{B}^4}{\bar{E}_x^4}\right), \quad (31)$$

$$\delta v_{\rm ref}(y) = \frac{\partial v_{\rm ref}}{\partial \boldsymbol{E}}\Big|_{\bar{\boldsymbol{E}},\bar{\boldsymbol{B}}} \cdot \delta\boldsymbol{E}(y) + \frac{\partial v_{\rm ref}}{\partial \boldsymbol{B}}\Big|_{\bar{\boldsymbol{E}},\bar{\boldsymbol{B}}} \cdot \delta\boldsymbol{B}(y). \quad (32)$$

By virtue of Eq. (30), we can rewrite $\delta v_{\rm ref}$ as

$$\delta v_{\rm ref} = -\sqrt{\frac{2q\bar{E}_x\Delta}{m}}\left[\left(\frac{1}{2} - \frac{3v_{\rm sh}^4}{8c^4}\frac{\bar{B}^4}{\bar{E}_x^4}\right)\frac{\delta E_x}{\bar{E}_x} + \frac{v_{\rm sh}^4}{2c^4}\frac{\bar{B}^4}{\bar{E}_x^4}\frac{\delta B}{\bar{B}}\right]. \quad (33)$$

The y-averaged $\delta v_{\rm ref}$ is zero.

Because $v_{\rm ref}$ varies along y, the fraction of reflected ions $n_{\rm ref}/n_0$ also depends on y. Extending Eq. (25) to this case, we have

$$\frac{n_{\rm ref}(y)}{n_0} \simeq \frac{1}{2}{\rm erfc}\left(\frac{v_{\rm ref}(y)}{\sqrt{2}v_{Ti}}\right). \quad (34)$$

We introduce the fraction of reflected ions in the 1D averaged fields, which is defined as

$$\frac{\bar{n}_{\rm ref}}{n_0} = \frac{1}{2}{\rm erfc}\left(\frac{\bar{v}_{\rm ref}}{\sqrt{2}v_{Ti}}\right). \quad (35)$$

Using Eq. (35), Eq. (34) is rewritten as

$$\frac{n_{\rm ref}(y)}{n_0} = \frac{\bar{n}_{\rm ref}}{n_0} + \frac{\delta n_{\rm ref}(y)}{n_0}, \quad (36)$$

where $\delta n_{\rm ref}(y)$ is given by

$$\frac{\delta n_{\rm ref}(y)}{n_0} = \frac{1}{\left(2\pi v_{Ti}^2\right)^{1/2}}\int_{\bar{v}_{\rm ref}+\delta v_{\rm ref}}^{\bar{v}_{\rm ref}} dv\exp\left(-\frac{v^2}{2v_{Ti}^2}\right). \quad (37)$$

When $\delta v_{\rm ref}$ is negative (positive), $\delta n_{\rm ref}$ is positive (negative).

We now consider the y-averaged value of $n_{\rm ref}/n_0$

$$\left\langle \frac{n_{\rm ref}}{n_0} \right\rangle \equiv \frac{1}{L_y}\int_0^{L_y} dy \frac{n_{\rm ref}(y)}{n_0}, \tag{38}$$

which is rewritten as

$$\left\langle \frac{n_{\rm ref}}{n_0} \right\rangle = \frac{\bar{n}_{\rm ref}}{n_0} + \left\langle \frac{\delta n_{\rm ref}}{n_0} \right\rangle. \tag{39}$$

Although the y-averaged $\delta v_{\rm ref}$ is zero, the y-averaged $\delta n_{\rm ref}$ is positive; that is, the second term in the right hand side of Eq. (39) is positive. This can be explained as follows.

We assume that $\delta v_{\rm ref}$ can be written as

$$\delta v_{\rm ref} = \delta v_1 \cos(k_y y + \alpha_y), \tag{40}$$

where δv_1, k_y, and α_y are constants, and $\delta v_1 > 0$ and $k_y L_y = 2\pi n$ with integer n are assumed. The maximum and minimum values of $v_{\rm ref}$ are

$$v_{\rm rmax} = \bar{v}_{\rm ref} + \delta v_1, \quad v_{\rm rmin} = \bar{v}_{\rm ref} - \delta v_1. \tag{41}$$

Figure 3 displays the ion velocity function. The shaded area shows the reflected particles. The upper panel is for $v_{\rm rmin}$, indicating that $\delta n_{\rm ref}/n_0$ enclosed by the red line is positive, whereas the lower panel is for $v_{\rm max}$, indicating that $\delta n_{\rm ref}/n_0$ enclosed by the blue line is negative. Because the absolute value of the former $\delta n_{\rm ref}$ is greater than that of the latter, we can expect that the y-averaged value of $\delta n_{\rm ref}$ is positive.

When $|\delta v_{\rm ref}|$ is much smaller than $\bar{v}_{ref}$, $\delta n_{\rm ref}/n_0$ can be approximated as

$$\frac{\delta n_{\rm ref}}{n_0} \simeq -\frac{1}{(2\pi v_{Ti}^2)^{1/2}} \exp\left(-\frac{\bar{v}_{\rm ref}^2}{2v_{Ti}^2}\right)\left(\delta v_{\rm ref} - \frac{\bar{v}_{\rm ref}}{v_{Ti}^2}\delta v_{\rm ref}^2\right). \tag{42}$$

Substituting Eq. (40) in Eq. (42) and integrating it with y, we have

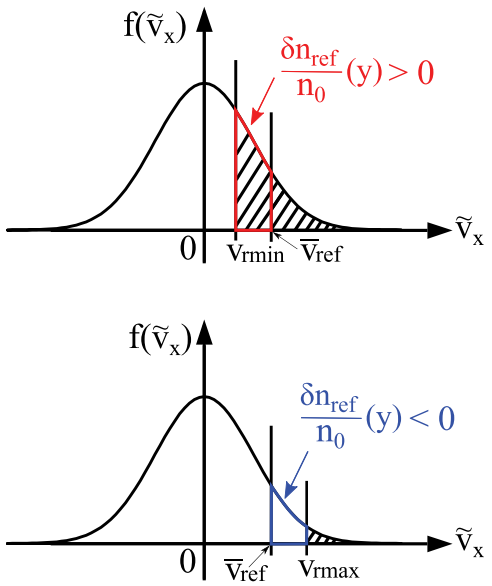

FIG. 3. Ion velocity distribution function $f(\tilde{v}_x)$. The reflected ions for $v_{\rm rmin}$ and $v_{\rm rmax}$ are represented by the shaded areas and are compared with the reflected ions for $\bar{v}_{\rm ref}$ in the 1D averaged fields.

$$\left\langle \frac{\delta n_{\rm ref}}{n_0} \right\rangle \simeq \frac{\bar{v}_{\rm ref}}{2\sqrt{2\pi}v_{Ti}^3} \exp\left(-\frac{\bar{v}_{\rm ref}^2}{2v_{Ti}^2}\right)|\delta v_1|^2 > 0. \tag{43}$$

Equations (39) and (43) lead to

$$\langle n_{\rm ref}/n_0 \rangle > \bar{n}_{\rm ref}/n_0. \tag{44}$$

We can also expect that as the amplitudes of the 2D electromagnetic fluctuations $\delta\boldsymbol{E}$ and $\delta\boldsymbol{B}$ increase, the fraction of reflected ions in the 2D electromagnetic fields becomes greater than that in the 1D averaged fields, $\bar{\boldsymbol{E}}$ and $\bar{\boldsymbol{B}}$.

IV. SIMULATION MODEL AND PARAMETERS

We study effects of trapped electrons on ion motion in an oblique shock wave using a 2D (two spatial coordinates and three velocity components) relativistic electromagnetic particle code with full ion and electron dynamics. The simulation system size is $L_x \times L_y = 16384\Delta_g \times 512\Delta_g$, where Δ_g is the grid spacing. The system is periodic in the y direction and is bounded in the x direction; the particles are confined in the region $200\Delta_g < x < L_x - 200\Delta_g$, being specularly reflected at these boundaries.[16] The shock wave propagates in the x direction in an external magnetic field in the (x, z) plane, $\boldsymbol{B}_0 = B_0(\cos\theta, 0, \sin\theta)$.

We choose the same values of parameters, except L_y, as those in Ref. 12, where the electron trapping and acceleration in an oblique shock wave were investigated in detail. The ion-to-electron mass ratio is $m_i/m_e = 400$. The light speed is $c/(\omega_{\rm pe}\Delta_g) = 4$. The ratio of $\Omega_{\rm e}$ to $\omega_{\rm pe}$ in the upstream region is $|\Omega_{\rm e}|/\omega_{\rm pe} = 5.0$. The Alfvén speed is $v_{\rm A}/(\omega_{\rm pe}\Delta_g) = 1.0$. The electron and ion thermal velocities are $v_{\rm Te}/(\omega_{\rm pe}\Delta_g) = 0.5$ and $v_{\rm Ti}/(\omega_{\rm pe}\Delta_g) = 0.025$. The plasma beta value is $\beta = 0.05$.

In order to elucidate the effects of 2D fluctuations on ion motions, we calculate orbits of test ions in the 1D averaged fields $\bar{\boldsymbol{E}}$ and $\bar{\boldsymbol{B}}$ obtained in the 2D electromagnetic particle simulation. We denote the test ions as 1Dt ions. The 1Dt ions do not feel the 2D fluctuations, $\delta\boldsymbol{E}$ and $\delta\boldsymbol{B}$. The number of the 1Dt ions is 4.1×10^6. We also follow the same number of ions in the 2D simulation, which we call 2Ds ions. The initial positions and velocities of the 2Ds ions are the same as those of the 1Dt ions. The fraction of the reflected 2Ds ions is $n_{\rm ref}/n_0$ and that of the reflected 1Dt ions is $\bar{n}_{\rm ref}/n_0$. We will show that y-averaged value of $n_{\rm ref}/n_0$, which is denoted by $\langle n_{\rm ref}/n_0 \rangle$, is greater than $\bar{n}_{\rm ref}/n_0$, as predicted in Sec. III.

V. SIMULATION RESULTS

A. Evolution of electrons and electromagnetic fields in an oblique shock wave

Before presenting the results on ion motions, we describe evolution of electrons and electromagnetic fields in an oblique shock wave. Figure 4 shows electron phase spaces (x, γ), x-profiles of $\bar{B}_z$, where $\bar{B}_z$ is y-averaged B_z, and contour maps of $\delta B_x = B_x - B_{x0}$ in the (x, y) plane at $\omega_{\rm pe}t = 520$ and 2320. The color in the phase space indicates the number density in the (x, γ) plane. At $\omega_{\rm pe}t = 520$, some electrons are

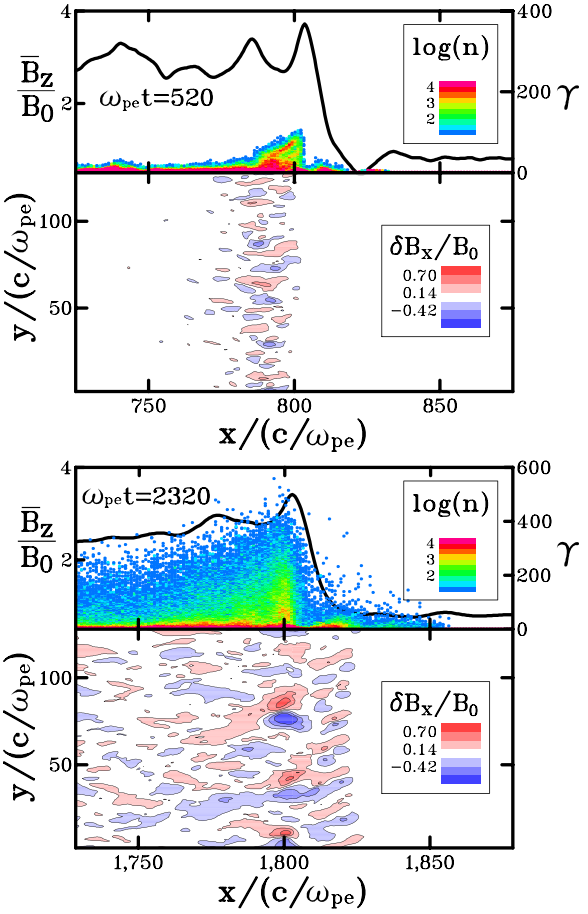

FIG. 4. Electron phase spaces (x, γ), x-profiles of $\bar{B}_z$, and contour maps of $\delta B_x = B_x - B_{x0}$ in the (x, y) plane at $\omega_{pe}t = 520$ and 2320.

reflected near the end of the main pulse and are energized there. The contour map of δB_x shows that 2D fluctuations are excited near the end of the main pulse. These fluctuations are due to oblique whistler waves excited by the reflected and trapped electrons. In the shock transition region $805 < x/(c/\omega_{pe}) < 810$, there are few trapped electrons and δB_x is negligibly small. At $\omega_{pe}t = 2320$, energetic electrons are distributed over the wide region from the upstream to the downstream of the shock wave. After trapping in the main pulse, some electrons are detrapped from it and are subsequently accelerated because of their gyromotions; this acceleration mechanism is the same as the mechanism for relativistic ions reported in Ref. 19. Compared to δB_x at $\omega_{pe}t = 520$, the 2D fluctuations at $\omega_{pe}t = 2320$ are excited in the wide range of x. Further, the amplitudes of δB_x in the main pulse region at $\omega_{pe}t = 2320$ are much greater than those at $\omega_{pe}t = 520$, as a result of nonlinear interaction of current filaments generated by the oblique whistler waves. The 2D fluctuations are also excited in the upstream region, which are due to the reflected ions (e.g., Refs. 17 and 18, and references therein). However, their amplitudes are much smaller than the 2D fluctuations due to the trapped electrons near $x = x_m$.

Figure 5 displays time variations of numbers of trapped and detrapped electrons and amplitudes of 2D electromagnetic fluctuations. The top panel shows the ratio N_{trap}/N_{enc}, where $N_{enc}(t)$ is the number of electrons that have

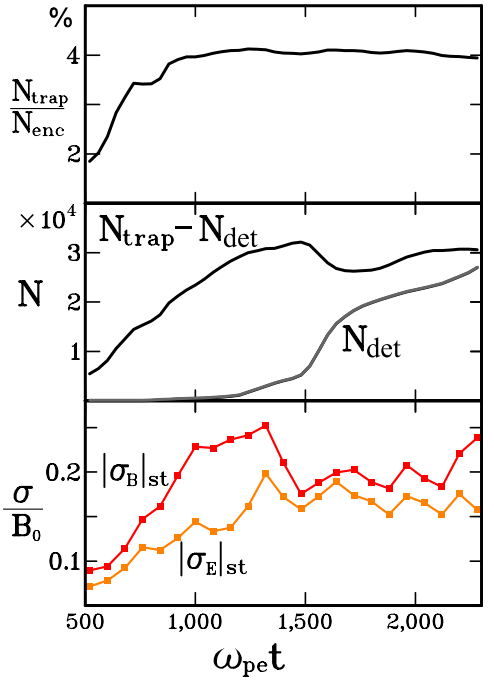

FIG. 5. Time variations of numbers of trapped and detrapped electrons, N_{trap} and N_{det}, and amplitudes of 2D electromagnetic fluctuations averaged over the shock transition region, $|\sigma_B|_{st}$ and $|\sigma_E|_{st}$. In the top panel, N_{trap} is normalized to the number of electrons that have encountered the shock wave, N_{enc}.

encountered the shock wave and $N_{trap}(t)$ is the number of electrons that have experienced trapping. The number of electrons that have been detrapped from the main pulse is denoted by N_{det}. The middle panel shows that the electron detrapping starts at $\omega_{pe}t \simeq 1000$. The bottom panel shows the magnitudes of 2D fluctuations. We define σ_B and σ_E as

$$\sigma_B(x,t) = \frac{1}{L_y}\sum_{j=x,y,z}\int_0^{L_y} dy|B_j(x,y,t) - \bar{B}_j(x,t)|,$$

$$\sigma_E(x,t) = \frac{1}{L_y}\sum_{j=x,y,z}\int_0^{L_y} dy|E_j(x,y,t) - \bar{E}_j(x,t)|. \quad (45)$$

The values of σ_B and σ_E averaged over the shock transition region are written as $|\sigma_B|_{st}$ and $|\sigma_E|_{st}$, that is,

$$|\sigma_B|_{st} = \frac{1}{\Delta}\int_{x_m}^{x_m+\Delta} dx\sigma_B(x,t), \quad |\sigma_E|_{st} = \frac{1}{\Delta}\int_{x_m}^{x_m+\Delta} dx\sigma_E(x,t). \quad (46)$$

Comparison between the middle and bottom panels shows that as $N_{trap} - N_{det}$ increases, both $|\sigma_B|_{st}$ and $|\sigma_E|_{st}$ increase. After $|\sigma_B|_{st}$ and $|\sigma_E|_{st}$ become large, the electron detrapping starts. At $\omega_{pe}t \simeq 1300$, $|\sigma_B|_{st}$, $|\sigma_E|_{st}$, and $N_{trap} - N_{det}$ are saturated.

We show the characteristic wavelength and frequency of the 2D fluctuations. Figure 6(a) shows the time variation of the wavelength along y, λ_y, of the dominant mode of δB_x in the main pulse. The values of λ_y are averaged over the period $\omega_{pe}t = 200$. (The wavelength along x, λ_x, is set to be almost equal to the width of the main pulse region because the 2D fluctuations have large amplitudes in this region. For the other λ_x, λ_y takes almost the same values of λ_y shown in Fig. 6(a).) At the initial stage ($\omega_{pe}t < 1000$), λ_y increases because of the nonlinear interaction of current filaments.

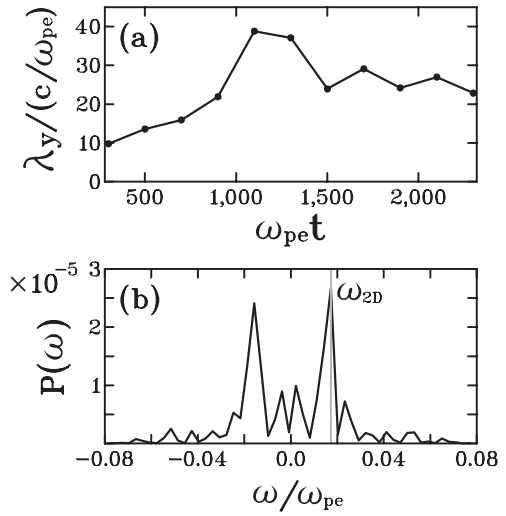

FIG. 6. (a) Time variation of the wavelength along y, λ_y, of the dominant mode of δB_x in the main pulse. (b) Frequency spectrum $P(\omega)$ of the mode with $\lambda_y \simeq 25c/\omega_{pe}$. The frequency at which $P(\omega)$ becomes maximum is defined as ω_{2D}.

Comparison of this figure with Fig. 5 shows that λ_y stops to increase when the electron detrapping starts. After $\omega_{pe}t = 1200$, λ_y oscillates with time. The value of λ_y averaged over the period from $\omega_{pe}t = 1500$ to 2500 is $\lambda_y \simeq 25c/\omega_{pe}$. Figure 6(b) shows the frequency spectrum $P(\omega)$ of the mode with this wavelength, $\lambda_y \simeq 25c/\omega_{pe}$. $P(\omega)$ has the peak at $\omega \simeq 1.7 \times 10^{-2}\omega_{pe}$ ($\simeq 1.4\Omega_i$, where Ω_i is the ion cyclotron frequency in the upstream region). We write this frequency as ω_{2D}.

B. Ion motion

1. Verification of assumption on 2D fluctuations in physical consideration

We first give an overview of ion motion in an oblique shock wave. Figure 7 shows the ion phase spaces (x, v_x) and (x, v_y), which are averaged over the y direction, and the x-profiles of $\bar{B}_z$ (black line in the top panel) and $\bar{\phi}$ (blue line) at $\omega_{pe}t = 920$, where $\bar{\phi}$ is the 1D averaged potential, defined as

$$\bar{\phi} = -\int_{x_0}^{x} dx \bar{E}_x(x). \tag{47}$$

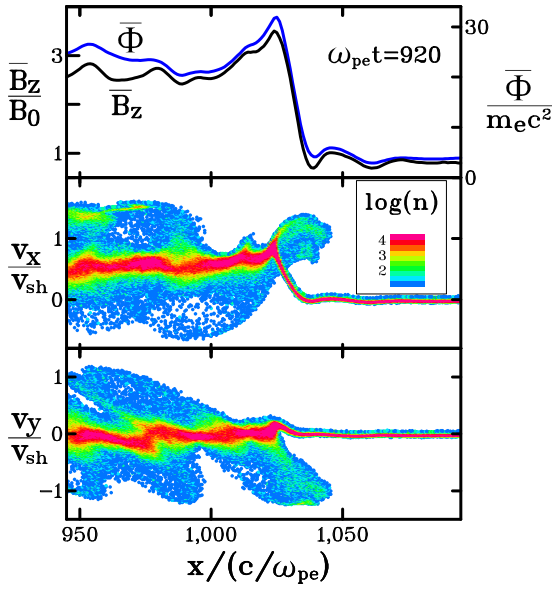

FIG. 7. Profiles of $\bar{B}_z$ and $\bar{\phi}$ and ion phase spaces (x, v_x) and (x, v_y) at $\omega_{pe}t = 920$.

Most of the ions transmit the shock transition region without reflection, whereas some ions are reflected from the shock front and go back to the upstream region. Because of the $\boldsymbol{v} \times \boldsymbol{B}$ force, the reflected ions change the direction of $\boldsymbol{v}$ and reenter the transition region. Then, they pass this region without reflection and go into the downstream region $x < x_m$. Unlike trapped electrons, reflected ions cannot stay near the shock front region for a long time. This is the reason why the amplitudes of instabilities due to reflected ions are much smaller than those due to trapped electrons, as shown in Fig. 4.

We next verify the assumption on the 2D fluctuations. In Sec. III, we assumed that the characteristic period of the 2D fluctuations is much longer than $t_{ref} - t_1$, where t_1 is the time at which an ion enters the shock transition region and t_{ref} is the ion reflection time. We also assume that characteristic wavelength of the 2D fluctuations, λ_y, is much greater than the displacement of the ion y during the period from t_1 to t_{ref}. Figure 8 displays time variations of $x - x_m$ and y of a reflected ion. Here, the time $t - t_1$ is normalized by T_{2D}, where T_{2D} is the characteristic period of the 2D fluctuation defined by $2\pi/\omega_{2D}$ with ω_{2D} shown in Fig. 6. The vertical gray lines indicate the times t_1 and t_{ref}, showing that $t_{ref} - t_1$ is much smaller than T_{2D}. The displacement of y during this period is $\Delta y \sim 3c/\omega_{pe}$. Comparison of this with Fig. 6 confirms that Δy is much smaller than the characteristic wavelength λ_y of the 2D fluctuations.

We also follow the orbits of many ions that enter the shock transition region during the period from $\omega_{pe}t = 1000$ to 2000 and obtain Fig. 9. The right panels show the

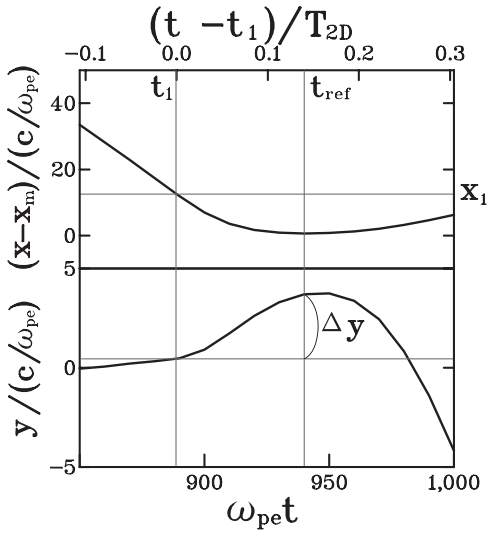

FIG. 8. Time variations of x and y of a reflected ion. The top axis is normalized by the characteristic period of the 2D fluctuations, $T_{2D} = 2\pi/\omega_{2D}$, where ω_{2D} was shown in Fig. 6.

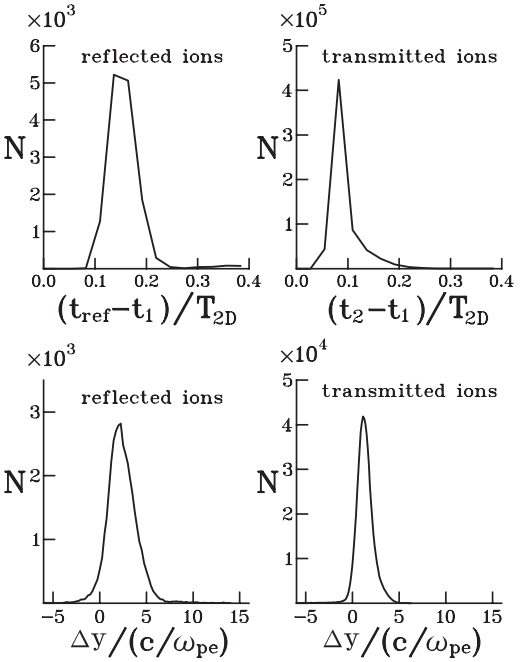

FIG. 9. Distributions of reflected ions as functions of $t_{\rm ref} - t_1$ and Δy for this period (left panels), and distributions of transmitted ions as functions of the time period in which ions transmit the shock transition region and Δy for this period (right panels).

distributions of reflected ions as functions of $t_{ref} - t_1$ and Δy. The left panels show the distributions of transmitted ions as functions of $t_2 - t_1$, in which ions transmit the shock transition region, and Δ_y for this period. For almost all the ions, $t_{\rm ref} - t_1$ and $t_2 - t_1$ are much smaller than T_{2D}, and the values of Δ_y for these periods are much smaller than λ_y. We thus confirm that the assumption in Sec. III is valid.

2. Effects of 2D fluctuations on ion motion

We now consider effects of 2D fluctuations on ion motion. To do this, we compare the 2Ds ions, which are under the influence of the 2D fluctuations, and the 1Dt ions, which are not. Figure 10(a) shows the x-profiles of $\bar{B}_z$ (black line), σ_B (blue), and σ_E (red) near the shock front at $\omega_{\rm pe}t = 520$, where σ_B and σ_E are the amplitudes of the 2D fluctuations defined by Eq. (45). The phase spaces (x, v_x) of 2Ds ions averaged over y and of 1Dt ions are shown in Figs. 10(b) and 10(c), respectively. The ions with $v_x > v_{\rm sh}$ in the region $x > x_m(\simeq 802c/\omega_{\rm pe})$ are reflected from the shock front. The fraction of such particles in the 2Ds ions, $\langle n_{\rm ref}/n_0\rangle$, is almost equal to that in the 1Dt ions, $\bar{n}_{ref}/n_0$. This is clearly shown in Fig. 10(d), where the distributions of 2Ds (black) and 1Dt (blue) ions in the shock transition region, $802 < x/(c/\omega_{\rm pe}) < 811$, are plotted as functions of v_x. The distributions of the two groups ions are almost the same. This is because at $\omega_{\rm pe}t = 520$, the amplitudes of the 2D fluctuations, σ_B and σ_E, are small in the shock transition region, although they are large near the end of the main pulse.

Figure 11 shows the same as in Fig. 10, except at $\omega_{\rm pe}t = 920$. At this time, the amplitudes of 2D fluctuations, σ_B and σ_E, are large near the center of the main pulse, unlike

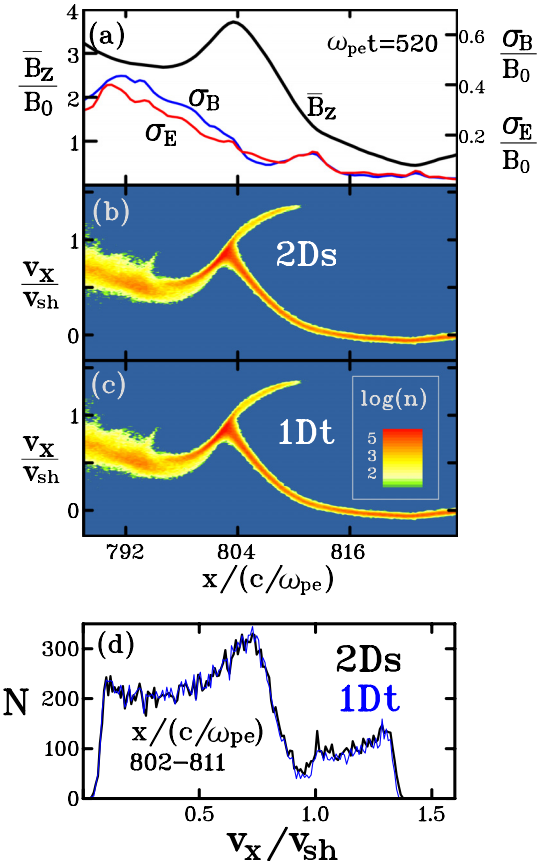

FIG. 10. (a) Profiles of $\bar{B}_z$ (black line) and amplitudes of 2D electromagnetic fluctuations, σ_B (blue) and σ_E (red) defined by Eq. (45), near the shock front at $\omega_{\rm pe}t = 520$, (b) phase space (x, v_x) of 2Ds ions, (c) that of 1Dt ions, and (d) distributions of 2Ds (black) and 1Dt (blue) ions in the shock transition region as functions of v_x.

at $\omega_{\rm pe}t = 520$. Because of these large-amplitudes fluctuations, there is a clear difference between the 1Dt and 2Ds ions. Some 2Ds ions are reflected from the shock front, whereas few 1Dt ions are. This is consistent with Eq. (43) indicating that as the amplitudes of 2D fluctuations in the shock transition region become large, more 2Ds ions are reflected, compared to the 1Dt ions.

We observe the time variations of electromagnetic fields and ion reflection in more detail. Figure 12 shows (a) the maximum value of $\bar{B}_z$, (b) the fraction of reflected 2Ds ions $\langle n_{\rm ref}/n_0\rangle$ (red) and the fraction of reflected 1Dt ions $\bar{n}_{ref}/n_0$ (blue), (c) their difference $\langle \delta n_{\rm ref}/n_0\rangle$, and (d) the amplitude of 2D fluctuations averaged over the shock transition region, $|\sigma_B|_{\rm st} + |\sigma_E|_{\rm st}$, where $|\sigma_B|_{\rm st}$ and $|\sigma_E|_{\rm st}$ are defined by Eq. (46). In the early stage $\omega_{\rm pe}t < 600$, the fraction of reflected 2Ds ions, $\langle n_{\rm ref}/n_0\rangle$, is almost equal to that of reflected 1Dt ions, $\bar{n}_{ref}/n_0$. However, after $\omega_{\rm pe}t > 800$, the former is much greater than the latter. The evolution of $\langle \delta n_{\rm ref}/n_0\rangle$ is roughly similar to that of $|\sigma_B|_{\rm st} + |\sigma_E|_{\rm st}$. We thus confirm that 2D electromagnetic fluctuations in the shock transition region can enhance the ion reflection. (More strictly, there are some differences between time variations of $\langle \delta n_{\rm ref}/n_0\rangle$ and $|\sigma_B|_{\rm st} + |\sigma_E|_{\rm st}$. This may be because $\langle \delta n_{\rm ref}/n_0\rangle$ also depends on $\bar{B}$ and $\bar{E}_x$, as suggested by Eqs. (31) and (43).)

Equation (33) indicates that the positive δE_x and δB enhance the reflection of 2Ds ions. We observe δE_x and δB

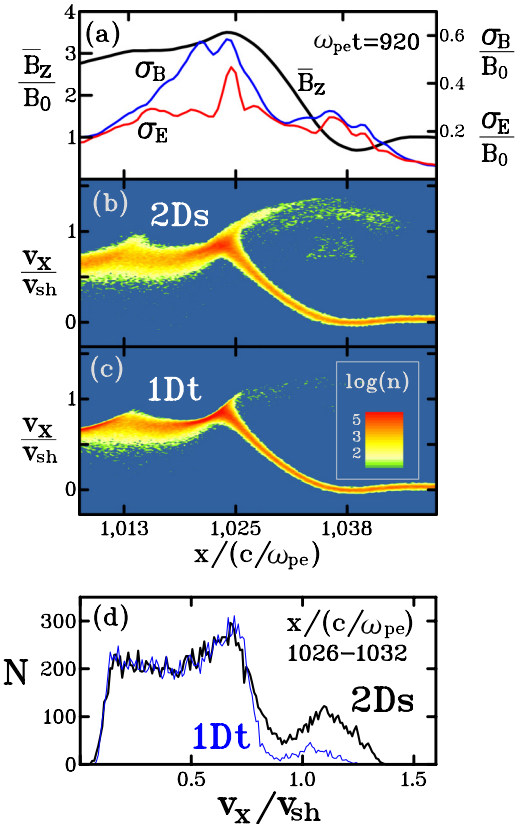

FIG. 11. The same as Fig. 10, except at $\omega_{pe}t = 920$.

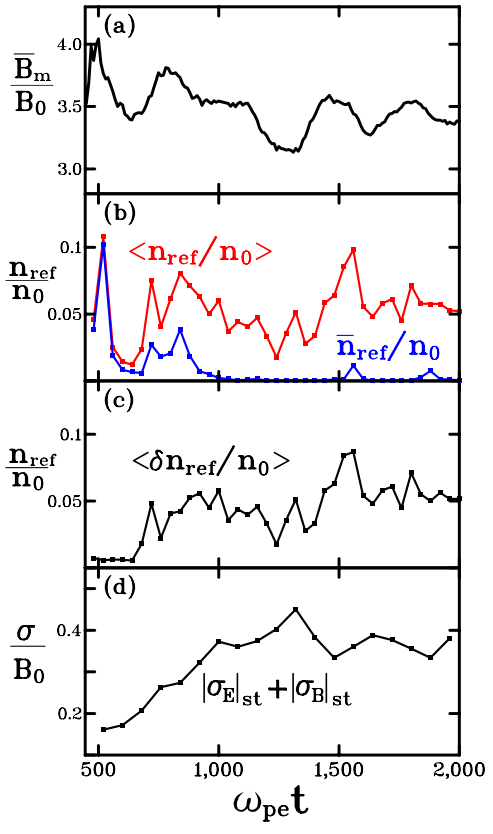

FIG. 12. Time variations of amplitude of electromagnetic fields and fractions of reflected ions: (a) the maximum value of $\bar{B}_z$, (b) the fractions of reflected 2Ds ions $\langle n_{ref}/n_0\rangle$ (red) and of 1Dt ions $\bar{n}_{ref}/n_0$ (blue), (c) their difference, $\langle \delta n_{ref}/n_0\rangle = \langle n_{ref}/n_0\rangle - \bar{n}_{ref}/n_0$, and (d) the amplitude of the 2D fluctuations in the shock transition region, $|\sigma_B|_{st} + |\sigma_E|_{st}$.

that the 2Ds ions felt before the reflection from $\omega_{pe}t = 1000$ to 2000. Figure 13 displays the distributions of reflected 2Ds ions as functions of δE_x and δB, where the values of δE_x and δB are averaged over the time from t_1 to t_{ref} for each reflected ion. This figure shows that most of the reflected ions felt the positive δE_x or the positive δB before the reflection.

C. Comparison with 1D simulation

We present results of the 1D simulation for the same parameters as the 2D simulation, except L_y and the total number of simulation particles. Figure 14 shows the maximum value of B_z, B_m, and the fraction of reflected ions n_{ref}/n_0 as functions of time. We see a clear correlation between B_m and n_{ref}/n_0; when B_m is large (small), the ion reflection is strong (weak). At some times, n_{ref}/n_0 is almost zero. However, as shown by the red line in Fig. 12(b) for the 2D simulation, the reflection of the 2Ds ions takes place continually. The time-averaged fraction of reflected ions from $\omega_{pe}t = 400$ to 2000 for the 2D simulation is 0.053, which is about 30% greater than that for the 1D simulation. A comparison between the top panels of Figs. 12 and 14 shows that the peak values of $\bar{B}_m$ in the 2D simulation are smaller than those of B_m in the 1D simulation after $\omega_{pe}t = 700$. This may indicate that the enhancement of ion reflection due to the 2D fluctuations influences the 1D averaged magnetic field and causes the reduction in $\bar{B}_m$. As a result of small peaks of $\bar{B}_m$ in the 2D simulation, the reflection of 1Dt ions, which are under the direct influence of $\bar{B}_m$, is considerably reduced after $\omega_{pe}t = 700$, as shown by the blue line in Fig. 12(b).

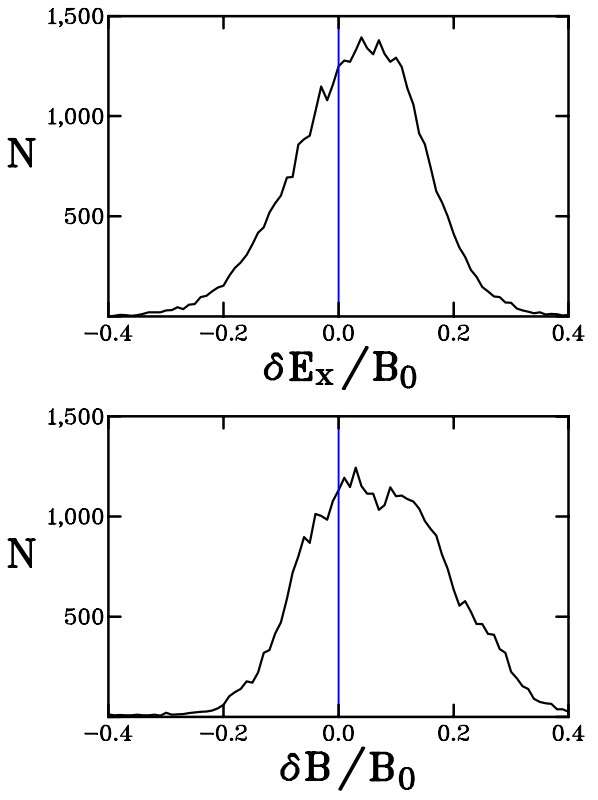

FIG. 13. Distributions of reflected ions as functions of δE_x and δB that the ions felt before the reflection.

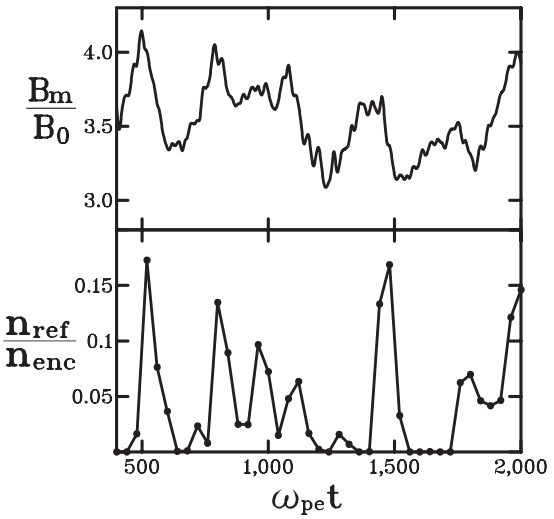

FIG. 14. Time variations of the maximum value of B_z and the fraction of reflected ions in the 1D simulation.

We next show that effects of trapped electrons on the ion reflection are negligible in the 1D simulation. Figure 15(a) shows the time variations of the number of trapped electrons $N_{\rm trap}$ (black) and its ratio to $N_{\rm enc}$ (gray). Figures 15(b) and 15(c) display the maximum values of $F(=-\int E_{\parallel}ds)$ and ϕ, F_m and ϕ_m, respectively. Figure 15(d) shows the value of B_y averaged over the shock transition region, $B_{\rm yst}$, where B_{yst} is defined by

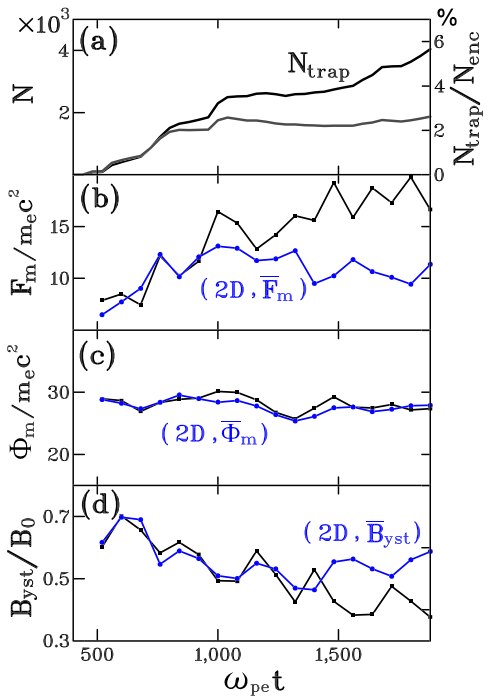

FIG. 15. Time variations of electrons and electromagnetic fields in the 1D simulation: (a) the number of trapped electrons and its ratio to the number of electrons that encountered the shock wave, (b) the maximum value of F, (c) the maximum value of Φ, and (d) the value of B_y averaged over the shock transition region. The blue lines in (b)–(d) show the values of the 1D averaged fields in the 2D simulation.

$$B_{yst}=\frac{1}{\Delta}\int_{x_m}^{x_1}B_y dx. \tag{48}$$

(F_m, ϕ_m, and $B_{\rm yst}$ in this figure are averaged over the period $\omega_{\rm pe}t=80$.) For comparison, the 1D averaged quantities in the 2D simulation, $\bar{F}_m$, $\bar{\phi}_m$, and $\bar{B}_{\rm yst}$, are plotted with gray lines, where $\bar{F}$ is defined as

$$\bar{F}=-\int\bar{E}_{\parallel}d\bar{s}=-\int(\bar{E}_{\parallel}\bar{B}/B_{x0})dx, \tag{49}$$

where $\bar{E}_{\parallel}=\bar{\boldsymbol{E}}\cdot\bar{\boldsymbol{B}}/\bar{B}$, $\bar{s}$ is the length along $\bar{\boldsymbol{B}}$, and $d\bar{s}=dx\bar{B}/B_{x0}$. As discussed in Sec. II, the increase in $N_{\rm trap}$ causes the increase in F_m and the decrease in B_{yst} in the 1D simulation. The increase in F_m indicates that $E_{\parallel}$ strengthens. However, Eq. (22) shows that the critical velocity for the ion reflection $v_{\rm ref}$ does not depend on $E_{\parallel}$, indicating that the change in $E_{\parallel}$ does not influence the ion reflection. The decrement in $B_{\rm yst}$ until $\omega_{\rm pe}t=2000$ is of the order of $0.1B_0$, which is much smaller than the amplitude of oscillation in B_m. Because of this, the change in B_y is also not important. Thus, the effects of trapped electrons on the ion reflection through the change in $E_{\parallel}$ and B_y are negligible in the 1D simulation. In the 2D simulation, $\bar{F}_m$ is saturated at $\omega_{\rm pe}t\simeq 1000$, at which the electron detrapping starts (see Fig. 5), and the decrement of $\bar{B}_{\rm yst}$ is smaller compared to that in the 1D simulation. The trapped electrons influence the ion reflection through exciting 2D fluctuations, which have the maximum amplitude of the order of B_0, as shown in Fig. 4.

VI. SUMMARY

A magnetosonic shock wave propagating obliquely to the external magnetic field can trap some electrons and accelerate them to ultrarelativistic energies. These electrons significantly influence electromagnetic fields near the shock front. In the 2D simulation, the trapped electrons excite whistler-wave instabilities. As a result of nonlinear development of the instabilities, 2D electromagnetic fluctuations along the shock front grow to large amplitudes. We studied effects of trapped electrons on ion motions in an oblique shock wave.

First, we analytically derived the condition for ions to be reflected from the shock front and the fraction of reflected ions, assuming that a shock wave propagates in the x direction in the external magnetic field, $\boldsymbol{B}_0=(B_{x0},0,B_{z0})$. It was predicted that the fraction of reflected ions is enhanced by the 2D electromagnetic fluctuations.

Next, we performed 2D electromagnetic particle simulations with full ion and electron dynamics. It was confirmed that 2D electromagnetic fluctuations are excited by trapped electrons. In order to study effects of the 2D fluctuations on ion reflection, we followed the orbits of a large number of ions (2Ds ions). We also calculated the orbits of the same number of test ions in the electromagnetic fields averaged along y. The test ions (1Dt ions) do not feel the 2D electromagnetic fluctuations. It was shown that the fraction of reflected 2Ds ions is greater than that of reflected 1Dt ions. The difference between the two groups of ions increases

with the amplitudes of the 2D electromagnetic fluctuations due to the trapped electrons. We also performed a 1D electromagnetic particle simulation. Although the trapped electrons strengthen $E_\parallel$ in the 1D case, the ion reflection is not significantly influenced by $E_\parallel$. The fraction of reflected ions in the 1D case is smaller than that in the 2D case.

ACKNOWLEDGMENTS

This work was carried out by the collaboration program, Grant Nos. NIFS14KNSS049 and NIFS14KNXN294 of the National Institute for Fusion Science and was supported in part by a Grant-in-Aid for Scientific Research (C) Grant No. 24540535 of Japan Society for the Promotion of Science.

APPENDIX A: DERIVATION OF EQUATIONS (7) AND (19)

In order to describe ion motion in the shock transition region $x_1 - \Delta < x < x_1$, we introduce the tensor T satisfying the relation

$$\boldsymbol{B}' = T\boldsymbol{B}, \tag{50}$$

where $\boldsymbol{B}'$ is

$$\boldsymbol{B}' = (0, 0, B). \tag{51}$$

When the magnetic field $\boldsymbol{B}$ is written as

$$B_x = B\sin\xi\cos\varphi, \quad B_y = B\sin\xi\sin\varphi, \quad B_z = B\cos\xi, \tag{52}$$

the components of T can be given by

$$T_{xx} = \cos\xi\cos\varphi, \quad T_{xy} = \cos\xi\sin\varphi, \quad T_{xz} = -\sin\xi, \tag{53}$$

$$T_{yx} = -\sin\varphi, \quad T_{yy} = \cos\varphi, \quad T_{yz} = 0, \tag{54}$$

$$T_{zx} = \sin\xi\cos\varphi, \quad T_{zy} = \sin\xi\sin\varphi, \quad T_{zz} = \cos\xi. \tag{55}$$

Using the tensor T, we also define $\boldsymbol{v}_0'$, $\boldsymbol{v}'$, and $\boldsymbol{E}'$ as

$$\boldsymbol{v}' = T\boldsymbol{v}, \quad \boldsymbol{v}_0' = T\boldsymbol{v}_0, \quad \boldsymbol{E}' = T\boldsymbol{E}. \tag{56}$$

Then, the equations of ion motion in the (x', y', z') frame are written as

$$m\frac{dv_x'}{dt} = qE_x' + \frac{q}{c}v_y'B, \tag{57}$$

$$m\frac{dv_y'}{dt} = qE_y' - \frac{q}{c}v_x'B, \tag{58}$$

$$m\frac{dv_z'}{dt} = qE_z' = qE_\parallel. \tag{59}$$

Provided that $\boldsymbol{E}'$ and $\boldsymbol{B}'$ are constant, the ion motion can be described by

$$v_x' = V_1\cos[-\Omega(t - t_1) + \eta_1] + cE_y'/B, \tag{60}$$

$$v_y' = V_1\sin[-\Omega(t - t_1) + \eta_1] - cE_x'/B, \tag{61}$$

$$v_z' = v_{\parallel 0}' + (qE_\parallel/m)(t - t_1). \tag{62}$$

Assuming that $\boldsymbol{v}'$ at $t = t_1$ is equal to $\boldsymbol{v}_0'$, we have V_1, η_1, and $v_{\parallel 0}'$ satisfying the relations

$$V_1\cos\eta_1 + cE_y'/B = v_{x0}', \tag{63}$$

$$V_1\sin\eta_1 - cE_x'/B = v_{y0}', \tag{64}$$

$$v_{\parallel 0}' = v_{z0}'. \tag{65}$$

The velocity $\boldsymbol{v}$ in the (x, y, z) frame is given by $\boldsymbol{v} = T^{-1}\boldsymbol{v}' = {}^tT\boldsymbol{v}'$. Therefore, we can write v_x as

$$\begin{aligned} v_x &= T_{xx}v_x' + T_{yx}v_y' + T_{zx}v_z' \\ &= V_1(T_{xx}\cos\psi + T_{yx}\sin\psi) + c(T_{xx}E_y' - T_{yx}E_x')/B \\ &\quad + T_{zx}v_{\parallel 0} + T_{zx}(qE_\parallel/m)(t - t_1), \end{aligned} \tag{66}$$

where

$$\psi = -\Omega(t - t_1) + \eta_1. \tag{67}$$

We can rewrite Eq. (66) as Eq. (7) as follows. Introducing V and η_2 given by

$$V = V_1\sqrt{T_{xx}^2 + T_{yx}^2}, \tag{68}$$

$$\cos\eta_2 = T_{xx}V_1/V, \quad \sin\eta_2 = -T_{yx}V_1/V, \tag{69}$$

we have

$$V_1(T_{xx}\cos\psi + T_{yx}\sin\psi) = V\cos(\psi + \eta_2). \tag{70}$$

Equations (55) and (56) lead to

$$\frac{c}{B}\left(T_{xx}E_y' - T_{yx}E_x'\right) = \frac{c}{B^2}(E_yB_z - E_zB_y). \tag{71}$$

We define v_{gx} and $\alpha_{\parallel x}$ as Eqs. (10) and (11), respectively. We also introduce η given by

$$\eta = \eta_1 + \eta_2. \tag{72}$$

Then, we rewrite Eq. (66) as Eq. (7). Using Eqs. (63), (64), and (69), we obtain $V\cos\eta$ and $V\sin\eta$ as Eqs. (8) and (9), respectively.

We now derive Eq. (19). We assume that $E_y \sim -v_{\rm sh}B_{z0}/c$ and $E_z \sim 0$ because E_y and E_z are equal to these values when the shock wave is 1D and stationary. We also assume that $B_z \gg B_y, B_x, B_0$ and $v_{\rm sh} \gg |\tilde{v}|$. Then, we can approximate

$$V\cos\eta \simeq -v_{\rm sh}, \tag{73}$$

$$V\sin\eta + \alpha_{\parallel x}/\Omega \simeq cE_x/B. \tag{74}$$

Substituting these in Eq. (17), we have

$$\psi_0 \simeq v_{\rm sh}B/(cE_x). \tag{75}$$

By virtue of Eqs. (73)–(75), Eq. (18) leads to

$$\delta \simeq -\frac{v_{\rm sh}^2}{2c^2}\frac{B^2}{E_x^2}. \tag{76}$$

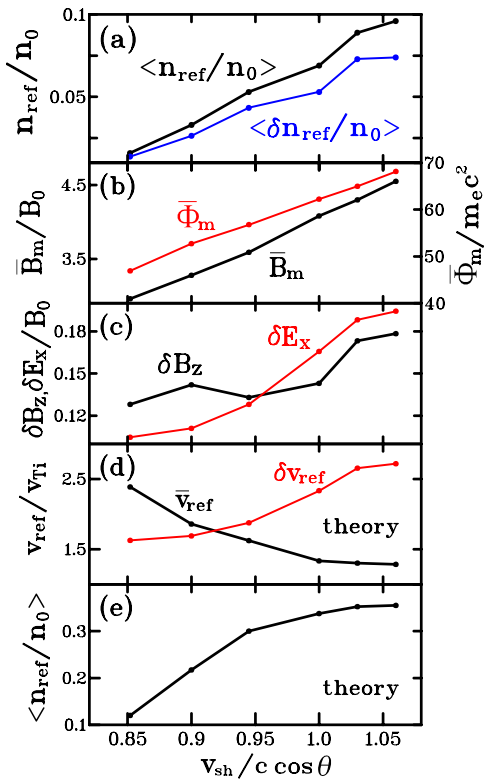

FIG. 16. Dependence of ion reflection and electromagnetic fields on v_{sh}: (a) the fraction of reflected 2Ds ions (black line) and the difference between the 2Ds and 1Dt ions (blue), (b) the maximum values of $\bar{B}_z$ (black) and $\bar{\Phi}$ (red), (c) the amplitudes of 2D fluctuations, δB_z (black) and δE_x (red), in the shock transition region, (d) the theoretical estimate of $\bar{v}_{\rm ref}$ (black) and $\delta v_{\rm ref}$ (red) given by Eqs. (31) and (33), respectively, and (e) the theoretical estimate of $\langle n_{\rm ref}/n_0\rangle$ given by Eq. (A1).

APPENDIX B: DEPENDENCE ON v_{sh}

We have performed 2D simulations for various values of $v_{\rm sh}/(c\cos\theta)$ near $v_{\rm sh}/(c\cos\theta) = 1$. Other parameters are the same as those in Sec. IV. Figure 16 shows the dependence of ion reflection and electromagnetic fields on $v_{\rm sh}$. These values are averaged over the period from $\omega_{\rm pe}t = 500$ to 2000. Figure 16(a) shows the fraction of reflected 2Ds ions $\langle n_{\rm ref}/n_0\rangle$ (black line) and the difference between the 2Ds and 1Dt ions $\langle \delta n_{\rm ref}/n_0\rangle$ (blue). As $v_{\rm sh}$ increases, both $\langle n_{\rm ref}/n_0\rangle$ and $\langle \delta n_{\rm ref}/n_0\rangle$ increase. The maximum values of $\bar{B}_z$ (black) and $\bar{\phi}$ (red) are plotted in Fig. 16(b), and the amplitudes of 2D fluctuations of E_x and B_z in the shock transition region, $|\delta E_x|$ (black) and $|\delta B_z|$ (red), are in Fig. 16(c). Substituting these values in Eqs. (31) and (33), we have $\bar{v}_{\rm ref}$ (black) and $\delta v_{\rm ref}$ (red) shown in Fig. 16(d). By virtue of Eqs. (35) and (43), we can write $\langle n_{\rm ref}/n_0\rangle$ as

$$\left\langle \frac{n_{\rm ref}}{n_0} \right\rangle \sim \frac{1}{2}\,\mathrm{erfc}\left(\frac{\bar{v}_{\rm ref}}{\sqrt{2}v_{Ti}}\right) + \exp\left(-\frac{\bar{v}_{\rm ref}^2}{2v_{Ti}^2}\right)|\delta v_r|^2. \qquad \text{(A1)}$$

Figure 16(e) shows the theoretical estimate of $\langle n_{\rm ref}/n_0\rangle$ given by Eq. (A1), in which the values of $\bar{v}_{ref}$ and $\delta v_{\rm ref}$ are substituted. Comparison between Figs. 16(a) and 16(e) shows that Eq. (A1) can qualitatively explain the observed $\langle n_{\rm ref}/n_0\rangle$ in the 2D simulation. However, this equation gives overestimate of $\langle n_{\rm ref}/n_0\rangle$. This is because in deriving Eq. (A1), we assumed that $\bar{v}_{\rm ref} \gg \delta v_{\rm ref}$, which breaks down as shown in Fig. 16(d).

[1]Y. Ohsawa, Phys. Rep. **536**, 147 (2014).
[2]C. S. Morawetz, Phys. Fluids **4**, 988 (1961).
[3]D. Biskamp and H. Welter, Nucl. Fusion **12**, 663 (1972).
[4]D. A. Tidman and N. A. Krall, *Shock Waves in Collisionless Plasmas* (Wiley-Interscience, New York, 1971).
[5]Y. Ohsawa and Y. Terashima, Publ. Astron. Soc. Jpn. **42**, 551 (1990).
[6]S. R. Kane, E. L. Chupp, D. J. Forrest, G. H. Share, and E. Riege, Astrophys. J., Lett. **300**, L95 (1986).
[7]D. B. McDonard and M. A. O. Van Hollelbeka, Astrophys. J., Lett. **290**, L67 (1985).
[8]N. Bessho and Y. Ohsawa, Phys. Plasmas **6**, 3076 (1999).
[9]N. Bessho and Y. Ohsawa, Phys. Plasmas **9**, 979 (2002).
[10]M. Toida and K. Shikii, Phys. Plasmas **16**, 112305 (2009).
[11]K. Shikii and M. Toida, Phys. Plasmas **17**, 082316 (2010).
[12]M. Toida and J. Joho, J. Phys. Soc. Jpn. **81**, 084502 (2012).
[13]A. Zindo, Y. Ohsawa, N. Bessho, and R. Sydora, Phys. Plasmas **12**, 052321 (2005).
[14]S. Takahashi and Y. Ohsawa, Phys. Plasmas **14**, 112305 (2007).
[15]T. Kawashima, S. Miyahara, and Y. Ohsawa, J. Phys. Soc. Jpn. **72**, 1164 (2003).
[16]P. C. Liewer, A. T. Lin, J. M. Dawson, and M. Z. Caponi, Phys. Fluids **24**, 1364 (1981).
[17]N. A. Krall and P. C. Liewer, Phys. Rev. A **4**, 2094 (1971).
[18]T. Umeda, Y. Kidani, S. Matsukiyo, and R. Yamazaki, Phys. Plasmas. **19**, 042109 (2012).
[19]S. Usami and Y. Ohsawa, Phys. Plasmas **9**, 1069 (2002).